

SENSITIVITY OF THE EARTHQUAKE RESPONSE OF A HDRB SEISMICALLY ISOLATED HOSPITAL TO LOCAL CRUSTAL EARTHQUAKES

José A. GALLARDO^{1,2}, Juan C. de la LLERA^{1,2}, Jorge G. F. CREMPIEN^{1,2}, Fabio FREDDI³, Tiziana ROSSETTO³, José CEMBRANO¹, Matías F. CHACÓN^{1,2,4}, Juan P. MUÑOZ², Fernando GUTIÉRREZ-URZÚA³ & Sahin DEDE³

Abstract: *Seismicity in Chile is strongly dominated by subduction megathrust events. Hence, the characteristics of ground motions other than those produced by these events are less known. Such is the case for the ground motions generated by crustal faults close to urban areas; one example is the San Ramon fault (SRF), which was recently declared as potentially active. This work addresses the sensitivity of the structural response of a High Damping Rubber Bearing (HDRB) seismically isolated hospital in downtown Santiago, Chile, to earthquakes generated on this Fault. The SRF lies at less than 15 kilometers away from the hospital and there is very little data on its seismogenic capacity and source parameters. Hence, physics-based synthetic earthquake simulations using front-end technologies and bounds for the source parameters are used to predict the impact of such event in the performance of this test structure. The earthquake source parameters considered as uncertain in this study are the event magnitude, average rupture velocity, and corner frequency. To minimize the number of parameter combinations, a median, an upper, and a lower bound value were selected for each parameter. A set of 16 synthetic ground motion realizations were generated for each parameter combination (27), leading to a total of 432 synthetic records for the analysis. The variability of these records, and the inelastic cyclic response of the HDRBs, are used to compute the expected variations in the earthquake response of the hospital. Building response parameters, such as maximum deformation and shear forces of the isolated layer, inter-story building drifts, and floor accelerations of the superstructure are used to characterize variability of the hospital response. It is concluded that despite the smaller magnitudes of crustal events relative to the subduction ones, they will control some of the response limit states for buildings closer than 15 km to the fault, such as this seismically isolated hospital.*

Introduction

Chile is located at the subduction convergence zone between the Nazca and South American plates. Thus, the seismicity of the country is highly dominated by subduction megathrust events, which have strongly influenced over the years the development of local seismic analysis codes and design standards (INN, 1996; INN 2013). After the M_w 8.8 Maule (Chile) earthquake in 2010, the sanitary authorities promoted the use of seismic isolation in new hospital designs (de la Llera et al., 2015; Simpson et al., 2018) with the aim of operational continuity after the earthquake. As a result, most of new hospitals currently incorporate seismic isolation. The preferred isolation technology has been High Damping Rubber Bearings (HDRBs).

Recently, however, Chilean seismologists have inferred that there is another seismic hazard for the capital city, Santiago, which was previously neglected, originated on a crustal fault known as the San Ramon Fault (SRF) that runs for about 35 km in the North-South direction (see Figure 1), and dipping East at an angle of about 55° (Diaz et al. 2014). This fault has been recently considered as potentially active (Armijo et al., 2010), and the impact of an earthquake generated on it for the structures of the metropolitan region of Santiago, is completely unknown.

¹ Department of Structural and Geotechnical Engineering, Pontificia Universidad Católica de Chile, Santiago, Chile, jogallardo@uc.cl

² Research Center for Integrated Disaster Risk Management (CIGIDEN), Santiago, Chile

³ Department of Civil, Environmental & Geomatic Engineering, University College London, London, UK

⁴ Centro Nacional de Excelencia para la Industria de la Madera (CENAMAD), Pontificia Universidad Católica de Chile, Santiago, Chile

Consequently, this paper explores the effect of such ground motions on a single seismically isolated emergency hospital in downtown Santiago (shown schematically in Figure 1), given the criticality of this facility after a potential earthquake. However, since there is no reliable data on the seismogenic capacity and source parameters of an event on the SRF, the problem is treated under a framework of uncertainty. The SRF presents a segmentation along its trace and a complex kinematics, and hence, the size of the largest expected event depends on the number of segments that can be engaged in the event (Armijos et al. 2010). This implies that the magnitude of the event is variable, as well as other parameters such as the corner frequency and rupture velocity.

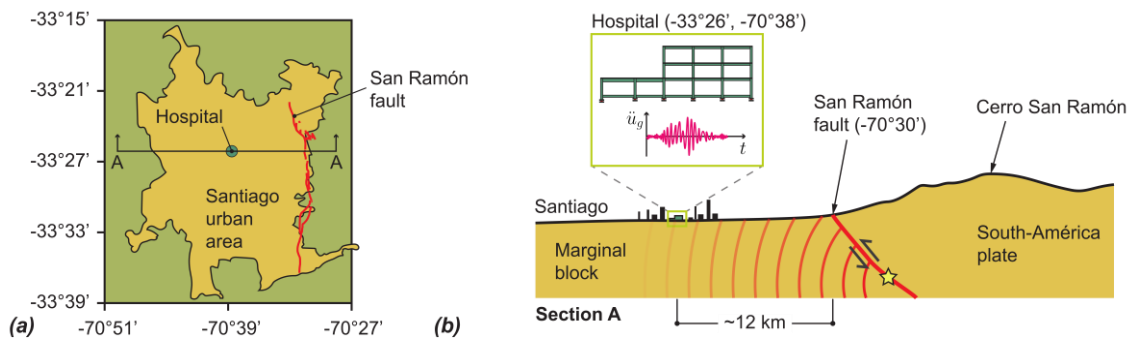


Figure 1. (a) Plan view of the Metropolitan region; and (b) schematic cross-section East-West, including a schematic representation of the San Ramon Fault

Because most of the new seismically isolated hospitals in Chile have been designed for a hazard defined by previous megathrust subduction events, the performance of these structures under the action of a crustal earthquake from the SRF is unknown. This work is based on the hypothesis that the probability for an event on the SRF is larger than zero, but it does not provide any additional evidence on the likelihood of such hypothesis. Herein, we assume that the hypothesis is true, and study the response of this hospital under such assumption. Naturally, the impact of a ground motion on the SRF affects all structures, not only hospitals; however, our research focus is to investigate the response of anear fault HDRB seismically isolated hospital under these conditions. Given the small distance between the structure and the fault, it is intuitive that the expected seismic performance of the structure could be affected. Crustal earthquakes may control some limit states of the structure and isolation system, which may condition the expected performance of the hospital.

Because of the lack of past data, this work addresses the sensitivity of the structural response of the hospital using synthetic earthquake signals generated from the SRF. To account for the uncertainty, median, upper and lower bound values for three key earthquake source parameters are considered, the magnitude of the event, the fault rupture velocity, and the corner frequency. These three parameters control important aspects of the synthetic earthquake signals.

Case-study

The San Ramón Fault (SRF) is located at the eastern border of Santiago, at the piedmont of the Andes mountain range (Díaz et al., 2014). It is a north-striking, west-verging, reverse fault that is part of the larger west Andean thrust system (Farías, 2007). The SRF trace has been defined by aligned topographic scarps of at least 35 km long following the mountain range foothills, extending from the Mapocho river in the north to the Maipo river in the south (Armijo et al., 2010, Rauld, 2011). Its trace is splitted in four segments, with a mean length of 10 km (Estay et al., 2016). Using fault trenching and cosmogenic isotope data, it was found that two large earthquake ruptures (M_w 7.5) occurred on the fault within the past 8000-19000 years, with displacements of ~5 m in each event (Vargas et al., 2014).

Besides its along-strike segmentation, the fault also has local kinematic complexity including normal, strike slip, and thrust subfaults, as well as potentially creeping regions, which reduces the magnitude of the largest expected event. The expected maximum event size it can generate for a thrust-type earthquake is of magnitude $M_w \sim 7.5$ (Vargas et al., 2014), whereas for a normal and strike-slip event, the maximum probable earthquake is of magnitude M_w 5.8. In the latter case the expected fault slip would be in the range between 20–80 cm.

Hospital Case-study

The history of this case-study hospital started August 7, 1911, with the creation of the first permanent and formal urgent care service in Santiago. The initiative was established by Dr. Alejandro del Rio, an iconic doctor of the public health system in the country. This landmark event was a transcendental moment in the consolidation of the modern medical assistance in the country. At the time police headquarters began to hire medical students to provide emergency healthcare responses in these quarters. This gave the name to this service as the Asistencia Pública (Public Assistance) to the injured. Moreover, the hospital was located in a very central location downtown Santiago, location that has been maintained over the years. By 1927, Santiago had 5 general hospitals for adults, 3 for children, and 3 for the new born. In 1993, the case-study hospital adopted a the new name of Urgent Care Hospital and Public Assistance, as it is known until today.

In 2013-2014, a revonation of the building was carried out. The new structure considered two neighbor Reinforced Concrete (RC) buildings; the principal with 2 basements and 3 stories, and based on structural frames and an isolation level that included rubber isolators and frictional sliders, conventional in-situ floor slabs of thickness 18 cm in the first basement, and posttensioned slabs in the second basement. The superstructure and substructure of this first building have a regular orthogonal grid of moment-resisting frames spaced at 8.00m; the substructure is buried and has very stiff retaining shear walls along the perimeter. On the other hand, the tower is a conventional structure and has a single basement and 7 stories with a heliport at the building roof. Building floor slabs are 15 cm thick, and the structure uses RC shear walls and beams, and steel members for the heliport. The structures are located in seismic Zone 2, and the foundation soil is the typical very stiff gravel of Santiago, classified as well as soil type 2 (INN, 2013). Concrete used in design was C25 grade with an uniaxial compressive strength of 25 MPa, and the reinforcement steel bars A630-420H grade with a yield stress of 420 MPa. This study focuses only on the seismic performance of the principal building, which is seismically isolated.

The seismic isolation system is located at the top of the two basements and consists of 33 HDRBs with a nominal shear stiffness $G = 4 \text{ kgf/cm}^2$, external diameter of 25 cm, and 19 frictional SLiders (SL) of diameters 35 and 45 cm with a total height of 28 cm. The nominal friction coefficient for the sliders at velocities exceeding 15 cm/s is between 5-7%. The design displacement for the isolators is 23.9cm, and the maximum total displacement 24.9 cm. Maximum axial stress for the sliders was 15 and 22 MPa for the long and short term loads, respectively. At the design displacement, the internal damping ratio for the rubber should exceed 9%, and the horizontal stiffness be in the range between 0.78 and 1.05 tonf/cm. Figure 2 shows a photograph of the isolated structure, the plan layout of the isolation layer, a typical elevation view of the structure and the schematic geometry of the HDRBs. The structural model omits the basements given their large stiffness.

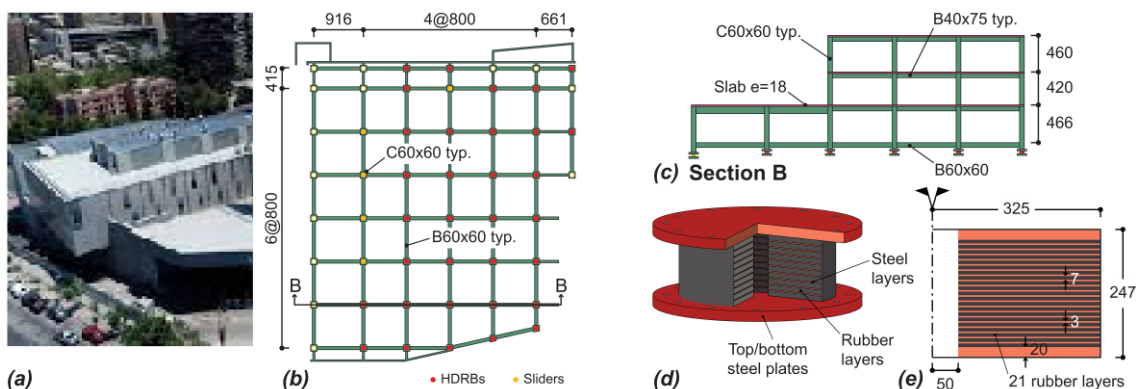


Figure 2. Case-study hospital building: (a) aerial view; (b) plan view of the isolation system; (c) typical elevation of the isolated structure; and (d - e) scheme of the HDRBs.

Structural and Ground Motion Modeling

This section describes the ground motion inputs considered and the structural model used for the analysis of the case-study. A total of 27 different cases for the earthquake source parameters

were considered, which together with the 16 realizations per case, give a total of 432 three-component ground motions.

Earthquake simulation

The ground motion is determined using the UCSB method (Liu et al., 2006; Schmedes et al., 2013; Crempien & Archuleta, 2015; Crempien & Archuleta, 2017), which involves simulating a synthetic earthquake source with specified temporal and spatial slip on the fault. To compute appropriate Green's functions for wave propagation away from the fault, the discrete wavenumber technique (Zhu & Rivera, 2002) is employed, which takes into account a 1D layered velocity structure.

The corner frequencies of the moment-rate spectra f_c and average rupture velocities V_r are varied, with the former being forced to have different values consistent with the scaling of this parameter with magnitude as proposed by Aki (1967), and the latter assumed independent of magnitude. The spatial characteristics of final slip, rise-time, peak-time, and rupture velocity on the fault are prescribed based on a von Kármán power spectrum correlation structure, with the parameters proposed by Crempien & Archuleta (2015) guiding the correlation structure of the rupture parameters. The fault dimensions are scaled using the relationship proposed by Leonard (2010), which yields lengths of 20, 30, and 50 km, and widths of 10, 16, and 25 km, for M_w 6.5, M_w 6.9, and M_w 7.2, respectively.

Case	M_w	V_r	f_c	Case	M_w	V_r	f_c	Case	M_w	V_r	f_c
1	6.5	2.5	0.12	10	6.9	2.5	0.07	19	7.2	2.5	0.05
2	6.5	2.5	0.14	11	6.9	2.5	0.09	20	7.2	2.5	0.07
3	6.5	2.5	0.16	12	6.9	2.5	0.11	21	7.2	2.5	0.09
4	6.5	3.0	0.12	13	6.9	3.0	0.07	22	7.2	3.0	0.05
5	6.5	3.0	0.14	14	6.9	3.0	0.09	23	7.2	3.0	0.07
6	6.5	3.0	0.16	15	6.9	3.0	0.11	24	7.2	3.0	0.09
7	6.5	3.5	0.12	16	6.9	3.5	0.07	25	7.2	3.5	0.05
8	6.5	3.5	0.14	17	6.9	3.5	0.09	26	7.2	3.5	0.07
9	6.5	3.5	0.16	18	6.9	3.5	0.11	27	7.2	3.5	0.09

Table 1. Ground motion cases considered in the analyses with variable moment magnitude M_w , rupture velocity V_r in km/s, and corner frequency f_c in Hz.

Table 1 shows the 27 cases considered in the parametric analysis. Each column of the table represents 9 cases, each column corresponding to a given earthquake magnitude M_w , which range from 6.5 to 7.2. Cases in rows are organized in ascending order of velocity of rupture V_r , ranging from 2.5 to 3.5 km/s, and corner frequency f_c varying between 0.05 to 0.16 Hz.

Structural modeling

A three-dimensional Finite Element (FE) model of the case-study was developed using OpenSees software (McKenna et al., 2000). The model includes all structural elements of the seismic isolation system and superstructure; the substructure was assumed rigid since it was buried in the ground and has large perimeter shear walls. Other assumptions of the model are: (i) fixity at the base of the isolation layer; (ii) a seismic mass equal to the self-weight plus 25% of the live-loads as specified by the Chilean code (INN, 1996); and (iii) a compatible mesh between all structural elements with a maximum element size of 1.5 m.

All elements in the superstructure were assumed elastic, as well as the response of the sliders. RC beams and columns were modeled using 2-node frame elements (*elasticBeamColumn*); slabs used a 4-node shell element (*ShellMITC4*) with an isotropic section (*ElasticMembranePlateSection*); sliders were modeled using 2-node link elements (*twoNodeLink*) with uniaxial elastic materials (*Elastic*) in each direction, and the HDRBs were modeled using a 2-node bearing element (*HDR*), which uses the model proposed by Grant et al. (2004) for simulating the shear response, and by Kumar et al. (2014) for cavitation under tensile loads. The response of the other three degrees of freedom and the axial response were considered linear and uncoupled. Figure 3 shows the FE model with the main assumptions, and an illustrative example of the shear force-deformation hysteresis of the HDRBs.

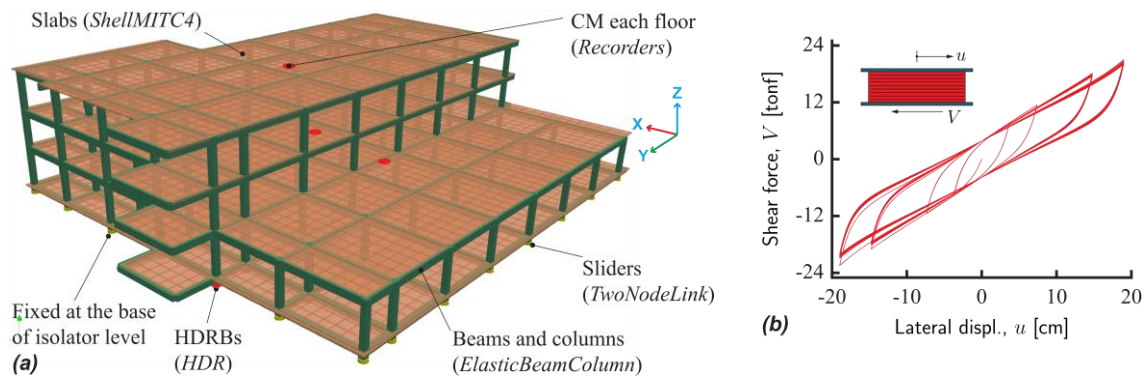


Figure 3. Case-study building: (a) 3D view of the FE model, and (b) shear force-lateral displacement hysteresis of the HDRB model.

The damping matrix of the superstructure was modeled using Rayleigh’s damping model, and neglects the contribution of the mass component to avoid damping leakage (Ryan and Polanco, 2008). This damping matrix is assumed to represent the energy dissipation capacity of the superstructure for a limited inelastic behavior of the elastic structural elements. A critical damping ratio of 2% at the natural frequency of the superstructure was chosen. Since the energy dissipation in the isolation layer is explicitly modeled, this damping is applied only to the superstructure. Thus, the *region* command was used to select all the elements of the superstructure and set the additional damping.

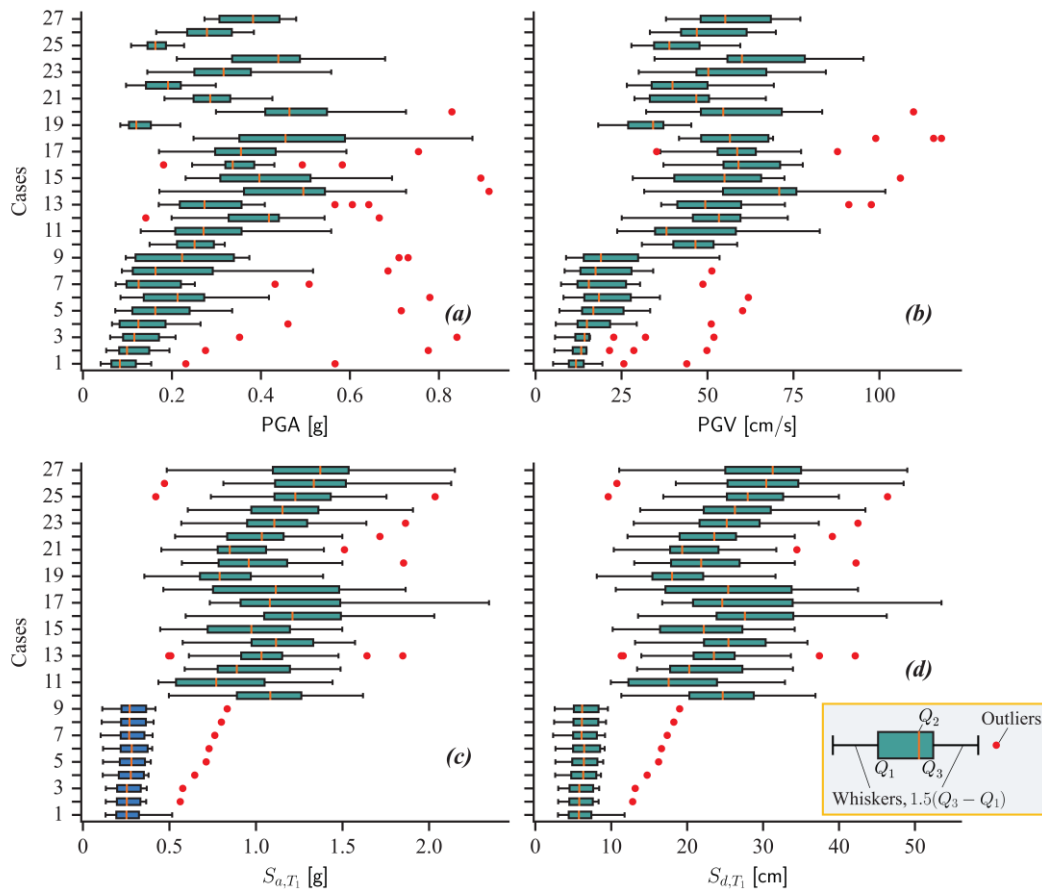


Figure 4. Boxplot for the different IMs considered: a) PGA; b) PGV; c) S_{a,T_1} , and d) S_{d,T_1} .

Results

Variability due to source parameters is characterized at two different levels. First, the different Intensity Measures (IMs) corresponding to the different earthquake source parameters are presented. Second, global and local building responses of the hospital are presented for the

different source parameters. The latter responses propagate the uncertainty represented by the bounds of the ground motion parameters into the building response.

Intensity Measures

Shown in Figure 5 are four different ground motion intensity measures for each of the 27 ground motion cases considered. The IMs included in this plot are the Peak Ground Acceleration (PGA), Peak Ground Velocity (PGV), pseudo-acceleration at the fundamental isolation period ($S_{a,T_1} = S_a(T_1)$), where $T_1 = 3.0$, and displacement at the same period of the latter variable ($S_{d,T_1} = S_d(T_1)$). The IMs are computed for the component oriented along the X-direction of the building. Each row in these plots represents the second quartile (Q_2) or median (orange vertical line); variability of the IMs (green box), which is the range between first (Q_1), median of the lower half of the data, and third quartile (Q_3), median of the upper half of the data; whiskers (black line segment), which extend the inter-quartile range ($Q_3 - Q_1$) 1.5 times; and the outliers (red circles), which are the values beyond the whiskers, for a given case.

The general trends for the IMs shown a marked jump between $M_w 6.5$ and $M_w 6.9$, while they are more gradual for the other magnitudes $M_w 6.9$ to $M_w 7.2$. As it should, the mean values of the IMs tend to increase as the magnitude of the event increases. The increase in PGA is more gradual and almost follows a linear trend up to $M_w 6.9$. Stronger discontinuities are observed for PGV, S_{a,T_1} and S_{d,T_1} as the system jumps from the $M_w 6.5$ to the $M_w 6.9$ earthquakes. Rupture velocity has also a significant effect in S_{a,T_1} and S_{d,T_1} for the larger magnitude $M_w 7.2$ earthquakes. For the $M_w 6.5$ case, the different rupture velocities do not affect significantly the median of the spectral intensity measures, though it does for the outliers. For the $M_w 6.9$ case, the effect of the rupture velocity on the PGA and PGV is smaller. Moreover, the effects of the corner frequency value are much clearly detected for the $M_w 7.2$ earthquakes and for the spectral IMs, S_{a,T_1} and S_{d,T_1} rather than for PGA and PGV. For a give rupture velocity, higher corner frequencies tend to produce larger median responses.

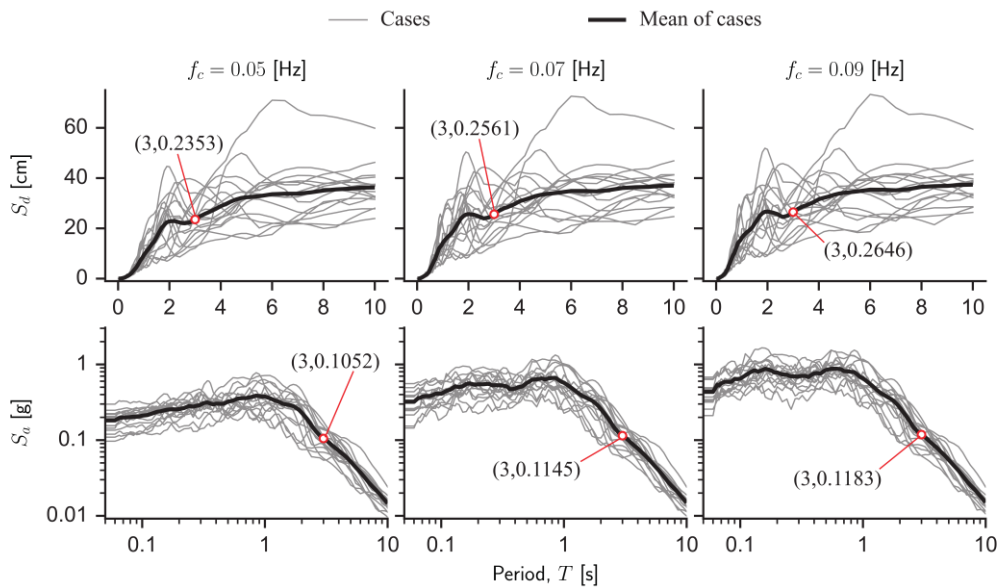


Figure 5. Effect of corner frequency for ground motion spectra with $M_w 7.2$, and $V_r = 3.0$ m/s.

Shown in Figure 5, are the S_a and S_d response spectra for the case $M_w 7.2$. The median values of S_a and S_d at the period of the structure do not seem to be influenced significantly by the corner frequency. However, detailed inspection of the amplitudes of the pseudo-accelerations show significant differences in the shorter period (higher frequency) range. The effect is less clear in the median of the pseudo-displacement S_d .

Analogously, Figure 6 presents similar results for the $M_w 7.2$ case, variable rupture velocity, and a given corner frequency, $f_c = 0.07$ Hz. In this case the effect of increasing the rupture velocity produces a clear increase on the displacement demand S_d at 3s. Given the frequency relationship between spectral values, the effect on S_a also exists and reaches close to 30% from the largest to the smallest rupture velocity.

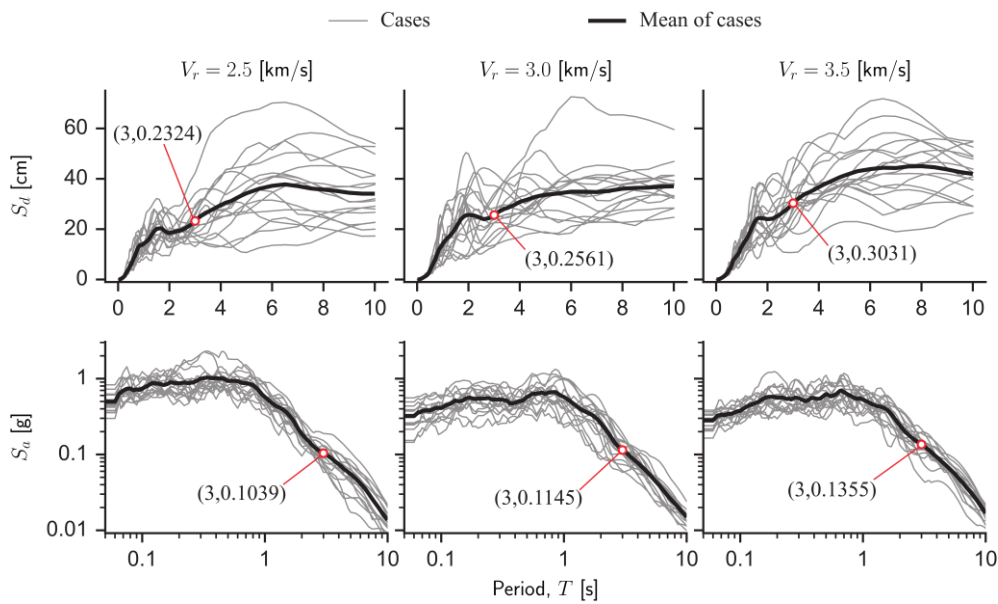


Figure 6. Effect of rupture velocity for ground motion spectra with M_w 7.2 and $f_c = 0.07$ Hz.

Structural response

The responses considered for the isolated interface of the hospital case-study are the displacements (u_i) and total shear force (V_i) of the isolation system. Building responses also include the inter-story drifts (Δ) and floor accelerations (\ddot{u}) in the superstructure. It is worth noticing that the response parameters are measured at the Center of Mass (CM) of each slab.

Shown in Figure 7 are the maximum displacements of the isolation system in the X-direction for the different ground motion cases, and the maximum X-direction shear force at the isolation level normalized by the total seismic weight (W) of the structure. The target displacement design value of 23.9 cm is presented as a vertical orange line in the figure, which is exceeded by some of the ground motion cases associated with the M_w 6.9 and M_w 7.2 earthquake scenarios. In the case of normalized maximum isolation shear force (V_{max}/W), it reaches maximum values beyond 30%, and typical values of about 20%. In all cases, the differences in response observed between the M_w 6.5 events and the M_w 6.9 ones are much larger than those occurring between M_w 6.9 and M_w 7.2. The responses for M_w 7.2 show in general larger median values than those of M_w 6.9. Results for M_w 7.2 also present larger dispersion than the other two cases. In general, the median values increase as, both, the corner frequency and rupture velocity increase.

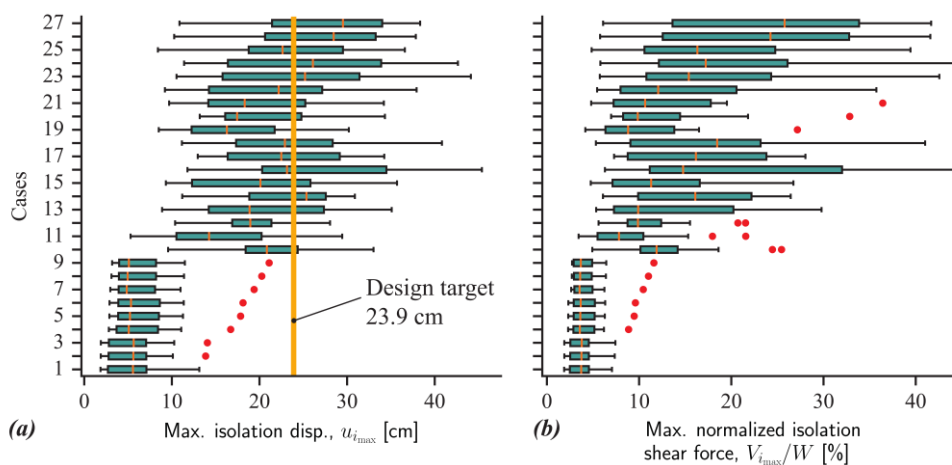


Figure 7. Boxplots for the demand parameters of the X-direction isolation system: a) maximum displacement $u_{i,max}$, and b) maximum normalized shear force $V_{i,max}/W$.

Figure 8 summarizes the maximum X-direction inter-story drifts (Δ_{max}) of the first and third stories, and the maximum X-direction floor accelerations (\ddot{u}_{max}) of the isolation slab and building roof.

Maximum drifts in the first-story may reach up to 8‰, and accelerations at the roof level up to 0.6 g. The general trends for both demand parameters of the superstructure are similar to those observed for the responses of the isolation system. Again, there is an important discontinuity between the demand for M_w 6.5 events and the other two magnitudes. In general, the responses for M_w 7.2 are larger than the other two cases. Increases in the corner frequency and average rupture velocity produce an increase in the demand on the superstructure.

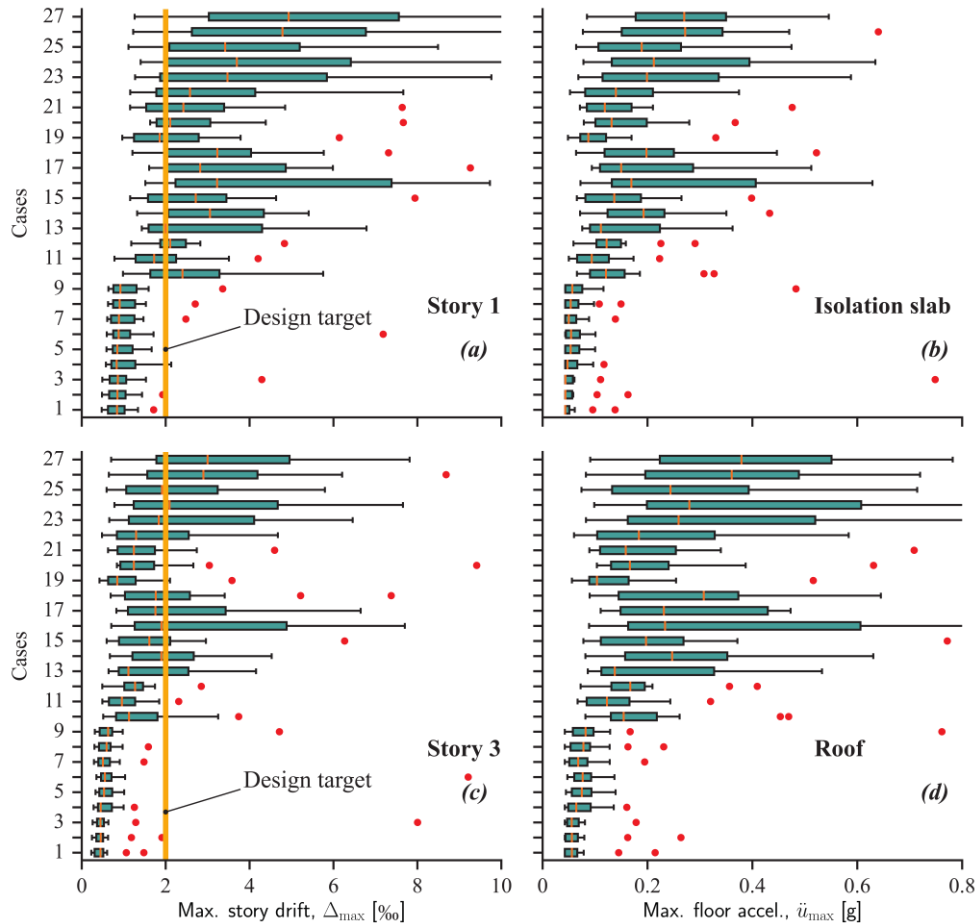


Figure 8. Boxplot for the demand parameters of the superstructure in X-direction: maximum inter-story drift Δ_{max} of: (a) first story; (c) third story ; and maximum floor accelerations \ddot{u}_{max} of (b) isolation slab, and (d) ceiling of third story (roof).

Limit states of the structure

The limit states chosen for the structure correspond to the maximum lateral displacement of the isolation system, and the inter-story drift target design value for the superstructure. For the isolation system, the critical components are the frictional sliders, whose maximum displacement is 28 cm. Thus, a displacement larger than this value would imply an impact between the slider and ring. For the superstructure, the design target of 2‰ for the inter-story drifts corresponds to a serviceability limit, since the structure can accommodate larger values of inter-story drift. Please recall that the 2‰ drift limit corresponds to the displacements for an R-factor reduced seismic load. The evaluation was performed considering the total displacement of the isolation system, and the total inter-story drifts in all three stories.

The probability of exceedance cases are presented in Figure 9. The cases with M_w 6.5 are not plotted since the displacement of the isolation system is always below the limit state, while for the inter-story drifts, eight of the nine cases shows probabilities of exceedance below 10%. The cases with M_w 7.2 present larger probabilities of exceedance than the cases for M_w 6.9. An increase in the average rupture velocity and the corner frequency imply a slight increase in the probability of exceedance of the isolation system limit state. For the superstructure, there is no clear trend, but the probability of exceedance is larger than 50% in all cases. This implies that the 2‰ drift condition will be exceeded almost surely for the M_w 6.9 and M_w 7.2 cases.

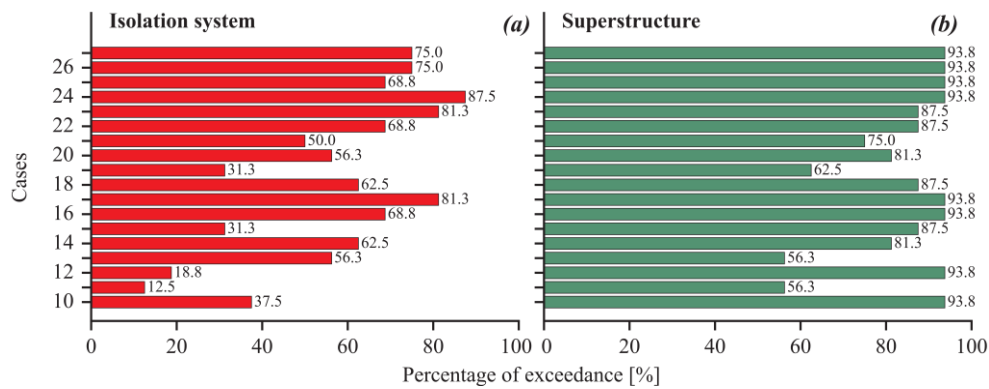


Figure 9. Probability of exceedance of two limit states for the different earthquake scenarios: (a) isolation system, and (b) superstructure.

Conclusions

This paper quantifies the dynamic response of an HDRB seismically isolated hospital in downtown Santiago for near fault ground motions occurring at the SRF. Since the parameters of the source are uncertain, bounds were proposed for the event magnitude, average rupture velocity, and corner frequency to account for the uncertainty of the earthquake source parameters. This uncertainty was propagated to the response of the hospital considered using all 27 possible combinations of parameters, with three magnitudes, three rupture velocities, three corner frequencies, and 16 realizations for each of the 27 cases. The effect of the different source parameters was evaluated for different ground motion IMs, i.e. PGA and PGV, and two dependent on both, the ground motion and the structural properties (S_{a,T_1} and S_{d,T_1}). In terms of structural response, four quantities were considered: the maximum lateral displacement and total shear force of the isolation layer in the X-direction, and peak X-direction inter-story drifts and floor accelerations at the isolation slab and roof of the superstructure. In this article, probabilities of exceedance were evaluated for two limit states, the maximum displacement of the isolation system (controlled by the frictional sliders), and the CM maximum elastic interstory drift limit specified by the Chilean code NCh433 for the reduced seismic load (2‰).

As it was expected, an increase in the magnitude of the event produces an increase in the IMs and demand on the structure. This increase is highly non-linear, and a large discontinuity was observed between the cases M_w 6.5 and M_w 6.9, which needs to be studied further. The increase in magnitude also increases the variability of the different realizations for each set of parameters. It was observed also that an increase in corner frequency and rupture velocity, increases the IMs and seismic demand on the structure. For all cases considered, the exceedance probability of the limit state considered for the deformation of the superstructure (2‰ drift) is larger than that for the isolation layer (28 cm of lateral displacement).

It is concluded that crustal earthquakes from the SRF may control the limit states of structures at 15km or less from the fault. This implies that under the hypothesis of an active fault, these structures should be evaluated under this new seismic hazard, and eventually consider a retrofit. The capacity reserve on a seismically isolated hospital like the one considered in this study is considerably larger than that of fixed-to-the-base buildings, which in some cases may even be closer to the SRF. These results are only a first attempt to quantify the effects of the SRF on existing buildings, they are not intended to cause any alarm since they are preliminary, but present also a word of caution for future designs in this zone to eventually avoid the need of future retrofits.

Currently, the authors are working on refining the sensitivity analyses of the impact of the earthquake source parameters of the SRF in this and other hospitals to present a more comprehensive proposal to different authorities and regulators. Future steps will include residential buildings at different distances from the SRF to define safer or even exclusion zones, the former requiring no building retrofit according to the current Chilean design practice.

Acknowledgements

This research has been sponsored by FONDECYT, under the project *Multiscale earthquake risk mitigation of healthcare networks using seismic isolation*, ANID/ FONDECYT/ 1220292 and ANID/doctorate scholarship/21201370, the Research Center for Integrated Disaster Risk

Management (CIGIDEN), ANID/ FONDAP/ 1522A0005; and the 2022 Seed Fund UCL-PUC research initiative. The authors are grateful for all this support.

References

- Aki K. (1967). Scaling law of seismic spectrum. *Journal of Geophysical Research*, 72(4), 1217-1231.
- Armijo R., Rauld R., Thiele R., Vargas G., Campos J., Lacassin R. and Kausel E. (2010). The West Andean thrust, the San Ramon fault, and the seismic hazard for Santiago, Chile. *Tectonics*, 29(2).
- Crempien J. and Archuleta, R. (2015). UCSB Method for Simulation of Broadband Ground Motion from Kinematic Earthquake Sources. *Seismological Research Letters*, 86, 61–67.
- Crempien J. and Archuleta R. (2017). Within-Event and Between-Events Ground Motion Variability from Earthquake Rupture Scenarios. *Pure and Applied Geophysics*, 174, 3451–3465.
- De La Llera J.C., Mitrani-Reiser J., Rivera J., Fortuño C., Jünemann R., Poulos A. and Vásquez J. (2015, November). The 2010 Chile earthquake: a five year reflection. In *Proceedings of the 10th Pacific Conference on Earthquake Engineering* (p. 210). AEES.
- Díaz D., Maksymowicz A., Vargas G., Vera E., Contreras-Reyes E. and Rebolledo S. (2014). Exploring the shallow structure of the San Ramón thrust fault in Santiago, Chile (~ 33.5 S), using active seismic and electric methods. *Solid Earth*, 5(2), pp.837-849.
- Estay N., Yáñez G., Carretier S., Lira E. and Maringue J. (2016). Seismic hazard in low slip rate crustal faults, estimating the characteristic event and the most hazardous zone: study case San Ramón Fault, in southern Andes. *Natural Hazards and Earth System Sciences*, 16(12), pp.2511-2528.
- Fariás M. (2007). Tectónica y erosión en la evolución del relieve de los Andes de Chile Central durante el Neógeno. Tesis de Ph.D. (Inédito), Universidad de Chile, Departamento de Geología: 191 p. In Spanish.
- Grant D., Fenves G. and Whittaker A. (2004). Bidirectional modelling of high-damping rubber bearings. *Journal of Earthquake Engineering*, 8(spec01), pp.161-185.
- INN (2013). NCh2745: Analysis and design of buildings with seismic isolation (In Spanish). *Instituto Nacional de Normalización*.
- INN (1996). NCh433: Earthquake resistant design of buildings (In Spanish). *Instituto Nacional de Normalización*.
- Kumar M., Whittaker A. and Constantinou M. (2014). An advanced numerical model of elastomeric seismic isolation bearings. *Earthquake engineering & structural dynamics*, 43(13), pp.1955-1974.
- Leonard M. (2010). Earthquake fault scaling: Self-consistent relating of rupture length, width, average displacement, and moment release. *Bulletin of the Seismological Society of America*, 100(5A), 1971-1988.
- Liu P., Archuleta R., and Hartzell S. (2006). Prediction of Broadband Ground-Motion Time Histories : Hybrid Low / High- Frequency Method with Correlated Random Source Parameters. *Bulletin of the Seismological of America*, 96, 2118–2130.
- McKenna F., Fenves G.L. and Scott M.H. (2000). Open system for earthquake engineering simulation. *University of California, Berkeley, CA*.
- Rauld R. (2011). Deformación cortical y peligro sísmico asociado a la falla San Ramón en el frente cordillerano de Santiago, Chile Central (33°s). Tesis de Ph.D. (Inédito), Universidad de Chile, Departamento de Geología: 311 p. In Spanish.
- Ryan K. and Polanco J. (2008). Problems with Rayleigh damping in base-isolated buildings. *Journal of structural engineering*, 134(11), pp.1780-1784.
- Schmedes J., Archuleta R., and Lavallee D., (2013). A kinematic rupture model generator incorporating spatial interdependency of earthquake source parameters. *Geophysical Journal International*, 192, 1116–1131.
- Simpson B., Kakoty P., Ortega M. and Hassan W. (2018). Resilience reconnaissance for hospitals after the 2010 Maule earthquake. *Technical report*.
- Vargas G., Klinger Y., Rockwell T., Forman S., Rebolledo S., Baize S., et al. (2014). Probing large intraplate earthquakes at the west flank of the Andes. *Geology*, 42(12), 1083–1086.
- Yáñez G., Perez-Estay N., Araya-Vargas J., Sanhueza J., Figueroa R., Maringue J. and Rojas T. (2020). Shallow anatomy of the San Ramón Fault (Chile) constrained by geophysical methods: implications for its role in the Andean deformation. *Tectonics*, 39(8), p.e2020TC006294.
- Zhu L. and Rivera L., 2002. A note on the dynamic and static displacements from a point source in multilayered media. *Geophysical Journal International*, 148(3), pp.619-627.